Check for updates

The Liquefaction and Cyclic Mobility Performance of Embankment Systems Constructed with Different Sand Gradations

Trevor J. Carey, Ph.D., A.M.ASCE[1]; Nathan C. Love[2]; and Jason T. DeJong, Ph.D., F.ASCE[3]

Downloaded from ascelibrary.org by University Of British Columbia on 07/31/23. Copyright ASCE. For personal use only; all rights reserved.

Abstract: A broad range of coarse-grained soils that vary in gradation uniformities, maximum particle sizes, and absolute densities are prone to liquefaction during earthquake shaking. However, clean, poorly graded sands form much of the liquefaction case-history database, with these soils often serving as the basis for analysis procedures. This paper presents a centrifuge testing program studying if the liquefaction triggering and deformation performance of embankment systems constructed with poorly graded sands universally applies to well-graded soils. Two soils were used in this study, named 100A and 25ABCD, had variations in maximum particle sizes, coefficients of uniformity (C_u), and void ratio extremes. Dense arrays of in-situ porewater pressure transducers and accelerometers indicate that liquefaction was triggered at near unity in the different soils. The 25ABCD soil, with its larger C_u and lower void ratio indices, exhibited stronger dilative tendencies, better preservation of the long period energy of the input motion, and more rapid dissipation of excess porewater pressures. The 25ABCD embankments had lower overall levels of strain at initial liquefaction triggering and accumulated less strain during cyclic mobility. While the two soils were pluviated to the same relative density and subjected to the same level of shaking, the slope surface displacements in the 25ABCD embankments were 60%–70% less than the displacements measured in the comparable 100A embankments. These results support the hypothesis that liquefaction and deformation behaviors depend on soil gradation, and findings from this experimental program can be leveraged for more accurate performance predictions of levees and earthen dams. **DOI: 10.1061/JGGEFK.GTENG-11501.** *© 2023 American Society of Civil Engineers.*

Author keywords: Liquefaction; Cyclic mobility; Centrifuge testing; Soil gradation; Well graded soils; Slope stability; Seismic embankment design; Earthquake shaking; Dynamic performance.

Introduction

The discipline's understanding of earthquake-induced soil liquefaction is largely informed by case-history observations collected following earthquakes over the last seventy years. Case histories serve as the basis for analysis procedures (Seed et al. 1983; Andrus and Stokoe 2000; Moss et al. 2006; Boulanger and Idriss 2015), inform laboratory studies of element behavior (Boulanger et al. 1998; Beyzaei et al. 2018), are vital for validation of numerical simulation tools (Gerolymos and Gazetas 2005; Bray and Macedo 2017), and often guide the design of system-level experiments (Horikoshi et al. 1998; Kutter 1992). Researchers use knowledge generated from case histories to infer the soil properties, state, and in-situ stress conditions conducive to liquefaction during an earthquake. Within the case history database, many of the observations of liquefaction are from sites where strata of clean, poorly graded fine- to medium-grained sands were determined to have liquefied during an earthquake (Boulanger and Idriss 2014). There are several interrelated factors for the overrepresentation of these sands, including prevalence near water bodies or prior use for hydraulic fill construction methods to build dams or for land reclamation (Seed et al. 1975; Ashford et al. 2004). In both cases, these sands are often very loose, making them highly vulnerable to liquefaction (Whitman 1971).

Clean, poorly graded sands do not represent all potentially liquefiable soils. Liquefaction has been observed in gravelly, or well-graded soils (Coulter and Migliaccio 1966; McCulloch and Bonilla 1970; Youd et al. 1985; Andrus 1994; Kokusho et al. 1995; Hatanaka et al. 1997; Lin et al. 2004; Cao et al. 2011; Cubrinovski et al. 2017), and researchers have used these case histories to create triggering curves (e.g., Cao et al. 2011; Ghafghazi and DeJong 2016; Rollins et al. 2021, 2022). Beyond triggering curves for gravelly, or well-graded soils, another analytical approach is to assume differences in the gradation properties of clean, poorly graded sands and well-graded soils are relative and use a clean, poorly graded sand procedure for all liquefiable soils. While a clean sand analysis procedure ignores the influence of soil gradation properties, this approach overcomes other challenges, such as an insufficient number of case history observations to generate unique triggering curves or the need to develop correlations for in-situ equipment suitable for testing large-diameter particles. Questions remain if the liquefaction triggering and the post-triggering deformation mechanisms developed for poorly graded fine sands universally apply to large grained-sands, gravelly, or well-graded soils vulnerable to liquefaction (e.g., with permeabilities <0.4 cm/sec allowing for the generation of excess porewater

[1]Assistant Professor, Dept. of Civil Engineering, Univ. of British Columbia, Vancouver, BC, Canada V6T 1Z4 (corresponding author). ORCID: https://orcid.org/0000-0003-4729-6884. Email: trevor.carey@civil.ubc.ca

[2]Graduate Student Researcher, Dept. of Civil and Environmental Engineering, Univ. of California at Davis, Davis, CA 95616. Email: nclove@ucdavis.edu

[3]Professor, Dept. of Civil and Environmental Engineering, Univ. of California at Davis, Davis, CA 95616. ORCID: https://orcid.org/0000-0002-9809-955X. Email: jdejong@ucdavis.edu

Note. This manuscript was submitted on November 22, 2022; approved on May 12, 2023; published online on July 27, 2023. Discussion period open until December 27, 2023; separate discussions must be submitted for individual papers. This paper is part of the ***Journal of Geotechnical and Geoenvironmental Engineering***, © ASCE, ISSN 1090-0241.

pressures, Roy and Rollins 2022). Fundamentally, the assumptions of liquefaction and deformation performance relate back to the interconnectivity of the excess porewater pressure behaviors and the transmissibility of shear stresses produced by accelerations.

This paper synthesizes the liquefaction and dynamic system-level performance of the two sands in the centrifuge test program described by Carey et al. (2022a). The testing program encompassed two centrifuge model tests of two parallel embankments in the same model container. The embankments were constructed with uniform profiles of two different test sands dry pluviated to a relative density (D_r) 63% for the first test and $D_r = 40\%$ for the second. The test sands utilized in this study are both poorly graded according to USCS classification; however, one test sand has void ratio indices and a coefficient of uniformity (C_u) that compares with sands more typical of the liquefaction case history database and prior research studies, while the other sand has lower void ratio indices and a larger C_u not typically found in liquefaction studies but often encountered in natural alluvial deposits. The more broadly graded soil was selected because its index properties (i.e., void ratio ranges and C_u) more closely align with gravelly or well-graded soils. The particle sizes of this test soil are smaller than gravels, but the soil skeleton and internal structure, which is a reflection of the broadness of the gradation (e.g., the void ratio indices and C_u) are more important than the actual particle sizes on the internal forces which influence soil behaviors (Santamarina 2003). A suite of soils ranging from poorly to well-graded will not have binary shifts in dynamic behaviors at changes of soil classifications, but rather, a gradient change as the soils become more well-graded. Trends and observations found through this study are expected to represent more broadly graded soils with larger particle diameters consistent with well-graded sands and gravels. Therefore, the background information will focus on well-graded or gravelly soils rather than the more well-understood poorly graded sand.

Background

The cyclic strength of well-graded or gravelly soils has been previously measured through a combination of integrated laboratory testing programs, system-level experimental testing, and case-history observations. These investigations have demonstrated strength and stiffness reductions during cyclic loading, causing shear strain accumulation, and often liquefaction. Linking these studies together is challenging because gradation or soil properties like grain size distributions, coefficients of uniformity, void ratio extremes, coefficients of curvature (C_c), mineralogies, or particle shapes have not been held constant among the different testing programs. These properties can vary significantly for well-graded soils due to the range of particle sizes.

Researchers have used laboratory testing to measure the cyclic strengths of gravelly or well-graded soils to assess the effect of gradation on cyclic resistance. Using cyclic triaxial testing, Wong et al. (1974) found that liquefaction resistance was higher for gravelly soils when compared with fine to medium-grained sands. However, they note that experimental findings may have been influenced by membrane penetration and quickly dissipating excess porewater pressures in the gravelly soil due to higher permeability. Vaid et al. (1990) performed a series of undrained cyclic triaxial testing on three soil gradations with the same D_{50} particle size, but with different C_u values. These tests indicated that cyclic strength increases with larger C_u values at low relative densities but an opposite trend was observed at high densities. Evans and Zhou (1995) constructed a series of gap-graded sand and gravel mixtures. Using a series of cyclic triaxial tests, they showed the gravelly mixtures had increased cyclic strength. In contrast, Kokusho et al. (2004) found that well-graded coarse-grained soils and poorly graded sands have similar cyclic strengths. Hubler et al. (2018) used a large-diameter cyclic simple shear device to test pea gravel, Ottawa C109 sand, and three intermediate pea gravel/sand mixtures. Through this testing, it was concluded that the soil skeleton (i.e., which particles participate in the load carrying structure) plays a pivotal role in the cyclic strengths of the different gradations. The conclusions from Hubler et al. (2018) agree with earlier observations by Siddiqi (1984), where they noted that a sufficient number of coarser particles are needed for particle-to-particle contacts. Xu et al. (2019) developed multiple sand-gravel mixtures with gravel contents varying from 0% to 80%. Using a large-scale direct simple shear device they showed three different phases of sandlike, transitional, and gravel-like with increasing gravel content. Each phase had distinct influences on cyclic strength.

There has been a limited number of centrifuge testing programs studying the dynamic behavior of gravelly or well-graded soils. Pires-Sturm and DeJong (2022) created a suite of composite sand gradations with median grain size diameters ranging from 0.13 to 2.58 mm and increasing C_u (1.7 to 7.8) by combining different proportions of four poorly graded sands sourced from the same geologic formation. Through a series of level-ground dynamic centrifuge tests, they found the composite gradations would all reach an excess porewater pressure ratio of 1.0 (r_u, where $r_u = \Delta u/\sigma'_{vo}$; Δu = is excess pore water pressure; and σ'_{vo} = initial vertical effective stress). Their testing showed the sand gradations with larger C_u values had more pronounced dilative behaviors and lower post-liquefaction reconsolidation volumetric strains. Another study by Ruttithivaphanich and Sasanakul (2022) created a composite gradation of 50% gravel and 50% sand and tested it using two level-ground dynamic centrifuge tests at a relative density of 10.2%. Liquefaction was triggered in these centrifuge model tests, and the acceleration and excess porewater pressure responses were similar to that of dense sand. These prior testing programs indicate that gravelly or well-graded soils may have similar dynamic behaviors as poorly graded sands but also indicate differences, specifically shear and volumetric strain accumulation during cyclic loading.

Recently, researchers have developed liquefaction triggering curves using case histories from sites consisting of gravelly or well-graded soils (Cao et al. 2011; Ghafghazi and DeJong 2016; Rollins et al. 2021, 2022). These relationships are typically formulated for penetration methods that are less influenced by the presence of large diameter particles (e.g., LPT, DPT, BPT, iBPT) or shear wave velocity measurements. One of the main drawbacks of any triggering curve is estimating deformation when liquefaction occurs. Liquefaction triggering for sand-based curves can be assumed when the $r_u = 1.0$ or at a single amplitude shear strain of 3%–3.5%, with both criteria often occurring in unity (Ishihara and Yoshimine 1992; Idriss and Boulanger 2008). It is not known whether the triggering or consequences of liquefaction in gravelly or well-graded soils differs from poorly graded sands because the current laboratory studies and system-level experiments have either lacked consensus or have been too narrow. Nonetheless, this issue is critically important as numerous geo-infrastructure systems are constructed with, founded on, or penetrate through gravelly or well-graded soils.

Centrifuge testing can be effectively used to experimentally investigate differences in the dynamic behavior of different gradation sands. Through this testing program, the input shaking demands, soil drainage conditions, dynamic behaviors, and deformation response can reasonably represent field conditions, which in turn can provide a deeper, systematic understanding of gradation effects.

Downloaded from ascelibrary.org by University Of British Columbia on 07/31/23. Copyright ASCE. For personal use only; all rights reserved.

Downloaded from ascelibrary.org by University Of British Columbia on 07/31/23. Copyright ASCE. For personal use only; all rights reserved.

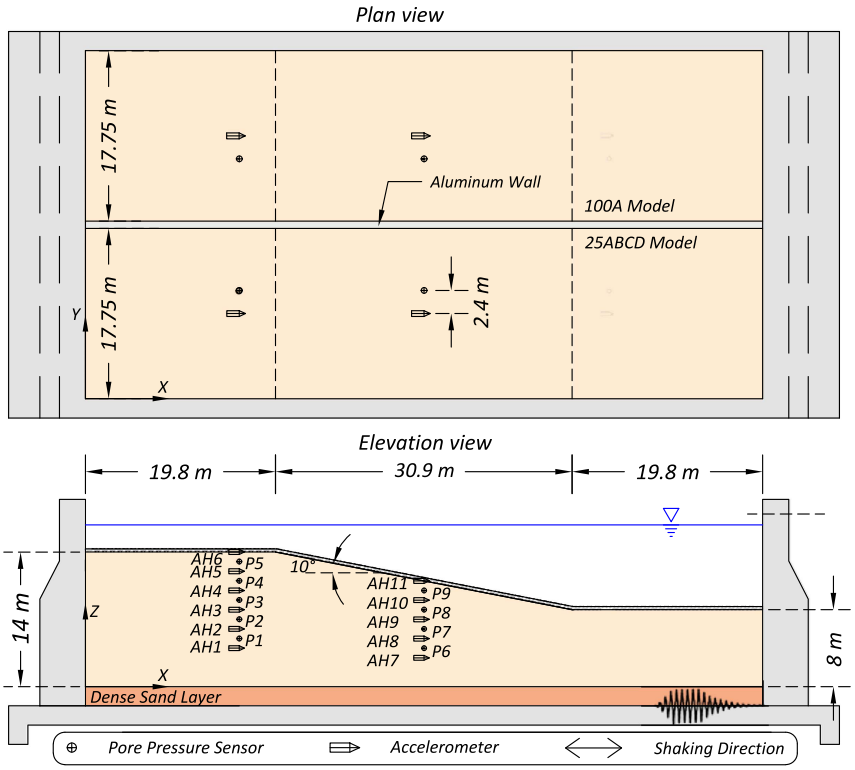

Fig. 1. Plan and elevation view of centrifuge model test geometry.

Experimental Test Program

Centrifuge testing was performed using the 9-m radius centrifuge at the University of California, Davis, Center for Geotechnical Modeling (CGM). The design of the centrifuge model test was two embankments parallel in the same model container, spun at 40-g following conventional centrifuge scaling laws (Garnier et al. 2007), and 1-dimensional shaking was applied at the base of the model container. Two experiments were conducted as part of this testing program. The only difference between the two model tests was the relative density of the sand used to construct the embankments, with one test being at $D_r = 63\%$ and the other at $D_r = 40\%$. Dense vertical arrays of accelerometers and porewater pressure transducers (PPTs) measured the in-situ dynamic response of the soil. High-speed cameras positioned exterior to the clear sidewalls of the model container recorded liquefaction-induced embankment deformations, with the experimental setup described in greater detail by Carey et al. (2022a). The dynamic performances of the embankments were evaluated using synchronous direct and processed time history measurements from accelerometers, PPTs, and high-speed cameras. The following description of model dimensions and testing results are in prototype scale unless otherwise noted.

The dynamic centrifuge model test configuration is given in Fig. 1. The model consisted of two parallel embankments, each with level ground segments that bounded a 10-degree slope. Each embankment was constructed with a different test sand, while the geometries and instrumentations were identical. The embankments were separated using a rigid wall that prevented dynamic interactions or drainage of excess porewater pressures. A layer of dense sand ($D_r > 90\%$) underlaid each embankment and elevated the model in the container for high-speed video recording. Beneath the level ground above the slope and in the midslope were vertical arrays of accelerometers and PPTs. The PPTs were offset from the accelerometers toward the center wall by 2.4 m to increase the vertical distance between sensors. A 0.3 m thick layer of permeable filter sand was added to provide 3–5 kPa of vertical effective confinement stress for the AH6 and AH11 surface accelerometers.

The grain size distributions and photos of the two test sands are given in Fig. 2. Sturm (2019) named, manufactured, and characterized the sand gradations for use in a centrifuge testing program. The 100A sand consists of US Silica New Jersey #70 sand, and the 25ABCD sand is equal parts by mass US Silica New Jersey #1, 3, 6, and 70 sands. Summarized in Table 1 are the physical and index properties of the sands, along with the permeabilities measured using a falling head permeability test in the laboratory. Pires-Sturm and DeJong (2022) provide additional information about the testing sands.

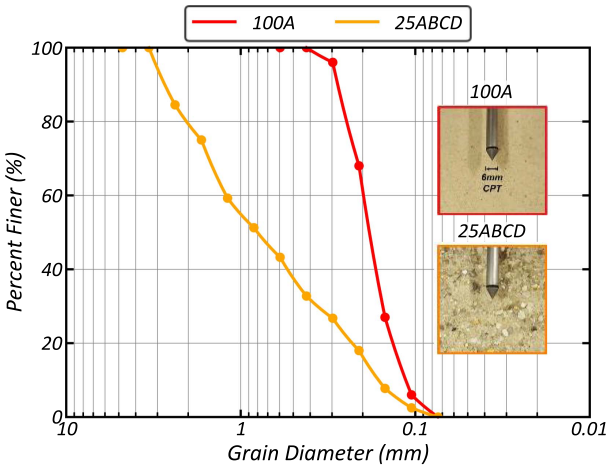

Fig. 2. Grain size distributions and photos of the test sands.

Table 1. Properties of the 100A and 25ABCD test sands at the testing densities

Sand	C_u	D_{10} (mm)	D_{50} (mm)	e_{min}	e_{max}	e @ $D_r = 40\%$	e @ $D_r = 63\%$	G_s	k @ $D_r = 40\%$ (cm/s)	k @ $D_r = 63\%$ (cm/s)
100A	1.68	0.12	0.18	0.579	0.881	0.76	0.69	2.62	0.025	0.020
25ABCD	7.44	0.16	0.8	0.303	0.544	0.45	0.39	2.61	0.022	0.013

The 100A and 25ABCD test sands are poorly graded (SP) per USCS classification [ASTM D2487 (ASTM 2017)]. The C_u (1.7) and void ratio extremes (0.58–0.88) of the 100A sand are similar to the sands used for prior liquefaction research studies (Arulanandan and Scott 1993; Robertson et al. 2000; Kutter et al. 2020b). Therefore, the embankments constructed with the 100A sand serve as a benchmark reference condition for liquefaction triggering and deformation behaviors of typical research sands. While the 25ABCD sand is also poorly graded, the gradation has a larger C_u (7.4) and a lower void ratio range (0.30–0.54) and is not typical of prior liquefaction research studies. It is reasonable to assume the test sands may have similar dynamic behaviors during earthquake shaking given they have the same soil classification, comparable permeabilities (i.e., 0.013–0.025 cm/s from Table 1), shape properties, and fabrics due to similar pluviation procedures.

For each centrifuge experiment, the embankments were constructed using dry pluviation by raining sand down from above the model container. The sand was pluviated in a series of 25.4 mm (1 in.) model scale lifts, which matched the vertical spacing between accelerometers and PPTs. The final 10-degree slope was created by placing a wooden template on the container and vacuuming the excess soil. Sensor locations and the final embankment geometry were validated using depth gauge measurements with an accuracy of 0.1 mm. The pluviation process was marginally adjusted for the different sands and relative densities to minimize construction differences that may impact experimental test findings. Specifics on the pluviation process, including equipment and sand drop heights, are summarized by Carey et al. (2021b, 2022b) for the two experiments.

The completed models were saturated following the procedure by Kutter et al. (2020a), which consisted of applying vacuum to the model, cycling between CO_2 and vacuum, and slowly dripping viscous pore fluid at the toe of the embankments for top-down saturation. The viscous pore fluid was hydroxypropyl methylcellulose mixed to a viscosity ($\mu*$) of 40 cSt to satisfy the scaling laws for diffusions and dynamic response (Kutter 1995).

Four, 1 Hz acceleration time histories simulated earthquake shaking. Each motion had the same topology, with successive phases where cyclic amplitudes were linearly increasing, constant, and decaying exponentially (Carey et al. 2022a). A single frequency accelerogram was preferred over complex frequency contents in an earthquake time-history record for interpreting the fundamental differences in soil behaviors. The peak ground accelerations (PGA) and the total number of loading cycles were increased later in the shaking sequence, resulting in higher seismic demands. The PGAs of the four motions ranged from 0.14 to 0.48 g for 7–20 cycles and Arias intensities (I_a) from 0.3 to 4.7 m/s. A minimum of 90 min of spinning time was given between each shake for the dissipation of excess porewater pressures. Fig. 3 presents the acceleration trace from the third shake in the ground motion sequence, which was 20 loading cycles with a PGA of 0.23 g and $I_a = 1.46$ m/s. The different phases of the input motion (i.e., build, hold, decay) are illustrated with different background shadings in Fig. 3. Additional information about the accelerogram design methodology and the repeatability of the

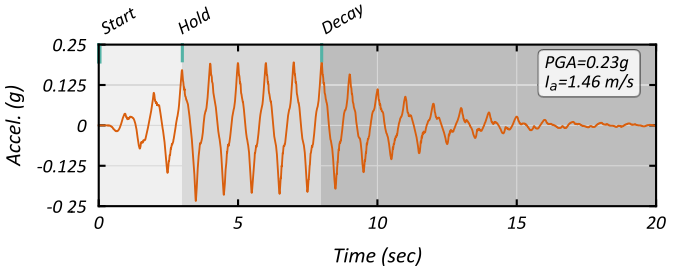

Fig. 3. Recorded input motion for shake #3 of the ground motion sequence.

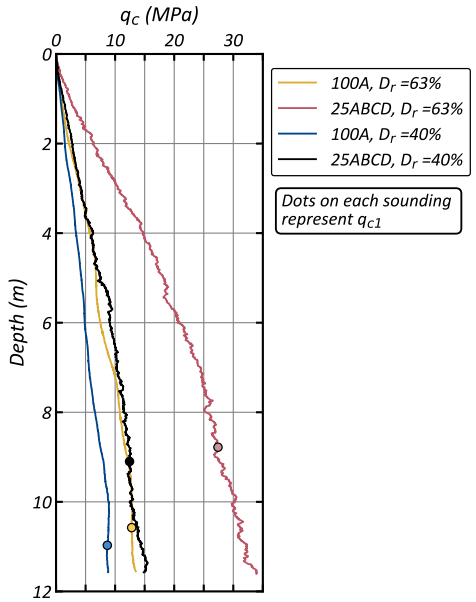

Fig. 4. CPT soundings measured before shaking in each embankment.

shaking between the two model tests is detailed by Carey et al. (2022a).

A 10 mm diameter cone penetrometer was pushed in each model before the first shaking event to characterize the initial properties of the embankments. In Fig. 4, the sounding profiles are given, with dots indicating the depth corresponding to one atmosphere of vertical effective confinement stress (q_{c1}) for that embankments. The overall shapes of the profiles are smooth with depth, which imply that the embankments were relatively uniform and free of significant loose or dense layers. While the models were constructed to the same relative density, the 25ABCD embankments had larger q_{c1} at both testing relative densities. The difference in q_{c1} measured in the 25ABCD sand were factors of 2.2 and 1.6 for the $D_r = 63\%$ and $D_r = 40\%$ models, respectively. Using CPT liquefaction triggering relationships by Boulanger and Idriss (2015), the cyclic

Downloaded from ascelibrary.org by University Of British Columbia on 07/31/23. Copyright ASCE. For personal use only; all rights reserved.

resistance ratios (CRR) for the 100A sand are estimated to be 0.19 and 0.12 for the dense and loose models. While for the 25ABCD sands, the CRRs computed from the triggering curve equation are 1950 and 0.19 for the same models. An estimated CRR of 1950 in the 25ABCD $D_r = 63\%$ model is beyond the mathematical bounds of the Boulanger and Idriss (2015) triggering relationships and should not be trusted without careful inspection; however, it is reasonable to assume liquefaction should not trigger.

Results

The characterization of the dynamic response of the embankments is achieved through measurements from accelerometers, PPTs, and deformations. These are independent measurements, but soil behaviors are interconnected, and responses typically occur synchronously. The traditional approach for analyzing centrifuge test data from different models is to compare time histories (Kutter et al. 2018). However, given the amount of data generated through this test program, it is not practical to present time histories from all shaking events from both model tests. The approach taken herein is presenting select time histories and synthesized data that demonstrate differences in the liquefaction and deformation response of the embankments. The following results are for shake 3 (input motion given in Fig. 3), but consistent trends were observed throughout the shaking sequence. Time histories for all shaking events are summarized by Carey et al. (2021a, b, 2022b).

Porewater Pressure Response

The excess porewater pressure response of the sands is demonstrated using the PPT measurements beneath the level ground segment above the slope. In Fig. 5, the r_u time histories for P5 (See Fig. 1 for location) are given for both sands and test densities. The abscissa axis in Fig. 5 has two timescales showing the generation and dissipation of excess porewater pressures. Excess porewater pressures accumulate rapidly, causing initial liquefaction ($r_u = 1.0$) to be triggered at near unity for all measurements. High r_u values were maintained through the duration of shaking and did not decrease until about 30 s. The excess porewater pressures dissipate faster in the 25ABCD sand for both densities. The postulated mechanism for this rapid dissipation in the 25ABCD sand is due to differences in the bulk modulus (K) of the two sands. Prior research efforts have shown that volumetric stiffness increases with soil density (e.g., Bray and Olaya 2022; Ishihara and Yoshimine 1992), supporting the theory of a larger bulk modulus. If the volumetric strain rates are equivalent in both sands, the larger K in the 25ABCD sand will produce a quicker reduction in excess porewater pressures during dissipation.

Fig. 6 provides the time durations between the first and last exceedance of $r_u = 0.5$ for all PPTs in the level ground array, with the measurements primarily being a comparison of dissipation times because the initial exceedances of $r_u = 0.5$ were nearly identical for equivalent depths, similar to P5 in Fig. 5. The curves in Fig. 6 remain parallel over the depth of the array. For the $D_r = 63\%$ test, r_u in the 25ABCD sand decreased to 0.5 in about 60% of the time measured in the 100A sand, and the ratio decreased to 45% for the $D_r = 40\%$ test. Rapidly decreasing r_u following earthquake shaking will reduce deformations. Adalier and Elgamal (2004) summarized prior research efforts and showed that as r_u exceeds 0.5–0.6, significant deformations begin to occur, with Howell et al. (2012) confirming their findings using prefabricated vertical drains to dissipate shaking-induced excess porewater pressures.

During shaking from 0 to 30 s, the excess porewater pressure responses in Fig. 5 show high-frequency spikes where the pressures rapidly decreased and rebounded. Kutter and Wilson (1999) described these spikes as de-liquefaction shockwaves which occur when the soil stiffens as it dilates, increasing shear stiffness and causing the upward propagating shear wave to transform into a sharp wavefront. These shockwaves, or dilation spikes, cause the soil to briefly deliquefy, restricting additional deformations.

The dilation spikes are an indicator of the dilatancy of the sands and are useful for delineating differences in dynamic behaviors. The number of dilation spikes that reduced excess porewater pressures below a r_u of 0.5 and the total duration of time below that threshold is presented in Fig. 7 for both sands and testing densities. Of the two test sands, the 25ABCD models had more dilation spikes and longer durations of reduced excess porewater pressures. Excess porewater pressures were less than a r_u of 0.5 for about 13.5% (2.61 s) of the shaking time in the 25ABCD sand in the $D_r = 63\%$ model. In contrast, in the 100A model for the same relative density, the spikes decreased the excess porewater pressures below a r_u of 0.5 for about 2% (0.43 s) of the shaking time. The 25ABCD sand had a closer grouping of individual dilation spikes, and hence, dilation was more periodic than the intermittent spikes in the 100A sand. These observations of porewater pressure response indicate

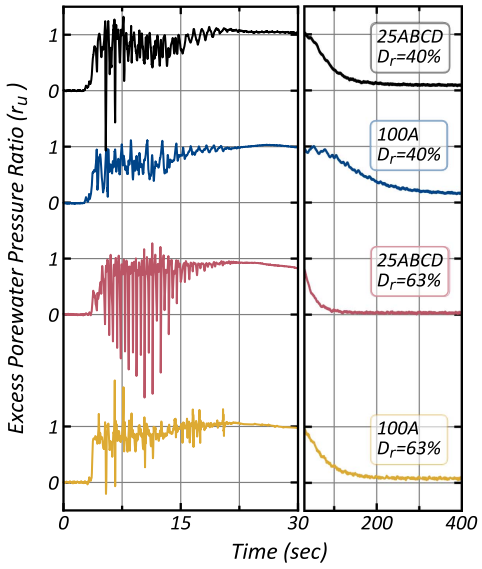

Fig. 5. Excess porewater pressures measured at P5 in each embankment.

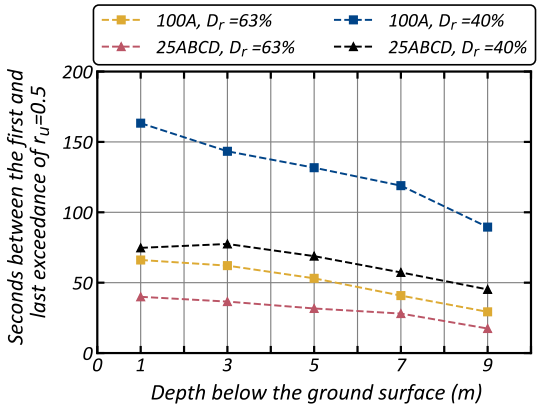

Fig. 6. Duration between first and last exceedance of $r_u = 0.5$ for the PPTs beneath the level ground.

Downloaded from ascelibrary.org by University Of British Columbia on 07/31/23. Copyright ASCE. For personal use only; all rights reserved.

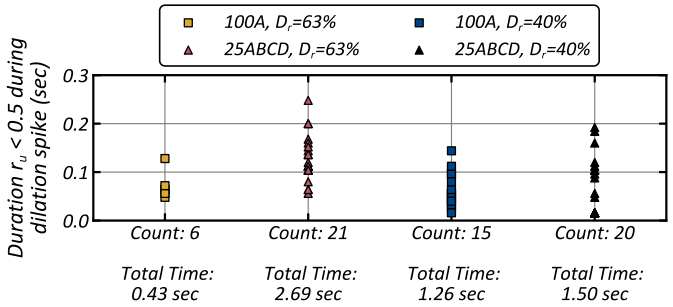

Fig. 7. Duration that dilation spikes were reduced $r_u < 0.5$, and cumulative time $r_u < 0.5$ for P5 from the dilation spikes.

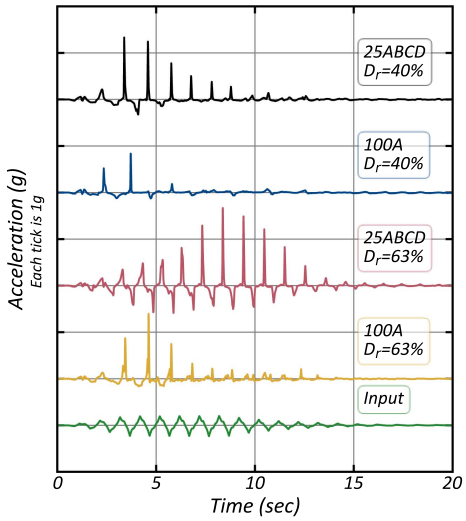

Fig. 8. Acceleration measured at AH6 in each embankment.

the embankments constructed with 100A sand should have greater deformation potential following the findings by Adalier and Elgamal (2004).

Acceleration Response

Acceleration measurements for the near-surface accelerometer (AH6) beneath the level ground are presented along with the input model container motion in Fig. 8 for both sands and test densities. All traces show a transformation from the input motion. It is apparent that the 25ABCD propagated shear stresses to the soil surface more strongly than the 100A embankments. The sharp spikes in acceleration occur simultaneously with the dilation spikes in the porewater pressure response in Fig. 5 and are caused by a wavefront from the stiffening soil during dilation (Kutter and Wilson 1999). More frequent spikes occurred in the 25ABCD sand for the two testing densities, consistent with the excess porewater pressure responses in Figs. 5–7. The flat acceleration response in the 100A sands shows that the soil could not transmit propagating shear stresses upward through the soil column, resulting in the accelerations being attenuated.

Response spectra are provided in Fig. 9 for the input container motion, AH4, AH5, and AH6, for both sands and relative densities. These spectra clearly show the differences in acceleration demands. The spectral responses from the in-situ sensors that bisect the gray shaded region have energy contents that are attenuated from the input motion at that period. The large spectral accelerations at short periods for all the responses in Fig. 9 are predominantly from the dilation spikes. In the 100A $D_r = 40\%$ response, there was attenuation of energy at the 1 s period input signal, and only minimal long period energy was measured at any of the accelerometers. The 100A sand in the $D_r = 63\%$ model better maintained stiffness during shaking and transmitted long period energy, but the spectral accelerations are elongated and attenuated from the 1 s period input motion and deamplification is greater closer to the ground surface. A similar attenuation occurred at the 1 s period input motion frequency in the 25ABCD $D_r = 40\%$ model. All spectral periods in the 25ABCD $D_r = 63\%$ model were amplified from the input motion, and the separation of the spectral acceleration curves have larger amplifications closer to the ground surface.

Deformation Response

Deformation at and following liquefaction triggering is one of the most important considerations during the seismic design of embankment systems. Both the porewater pressure and acceleration responses in Figs. 5–9 indicate that liquefaction was triggered when r_u approached a value of 1.0, but this does not translate to similar levels of deformation. The faster dissipation of excess porewater pressures coupled with the more frequent and intense dilation spikes in the embankments constructed with 25ABCD sand decreases the time the soil is at a liquefied state and most susceptible to deformations.

Embankment deformations were measured using a combination of in-situ sensors and high-speed video recordings. Permanent deformations were measured using high-speed cameras positioned on the exterior of the model container along the clear sidewalls using the hardware described by Carey et al. (2022a). The image correlation software, GEOPIV-RG (White et al. 2003; Stanier et al. 2016), was used to convert the videos into strain and displacement time histories. The complete length of the embankments could not be recorded due to physical space constraints and the need for many cameras for high-resolution images. Therefore, recordings were prioritized for the slope and portions of the level ground segments. Transient deformations during shaking were calculated for pseudo-elements located between vertically adjacent in-situ accelerometers in the sensor arrays using the inverse analysis procedures described by Kamai and Boulanger (2009) and the weighted residual by Brandenberg et al. (2010). A procedure developed by Carey et al. (2023) was used to combine transient strains from inverse analysis procedures and permanent strains from cameras to create composite time histories. The procedure uses a complementary filter with a crossover frequency of 0.4 Hz to eliminate double counting of measurements. Displacement measurements were verified using rulers and depth gauges to ensure they reasonably matched the values measured using cameras.

Lateral displacements and strains from shake 3 are shown in the contour diagrams in Fig. 10, with an outline of the embankment geometry. The measurements in Fig. 10 were made following the dissipation of excess porewater pressures after shaking had ended. The patterns of displacements and strains are consistent for both sands and relative densities, but the magnitude of displacement is less for the 25ABCD models. In the $D_r = 63\%$ experiment, the midslope surface displacement in the 25ABCD embankment was 0.09 m, compared to the 0.31 m for the 100A embankment. Throughout the height of the models, the displacements were about 1/3 the magnitude in the 25ABCD embankments compared to the 100A embankments at the same relative density. For the $D_r = 40\%$ model, larger displacements were measured in both soils.

Downloaded from ascelibrary.org by University Of British Columbia on 07/31/23. Copyright ASCE. For personal use only; all rights reserved.

Downloaded from ascelibrary.org by University Of British Columbia on 07/31/23. Copyright ASCE. For personal use only; all rights reserved.

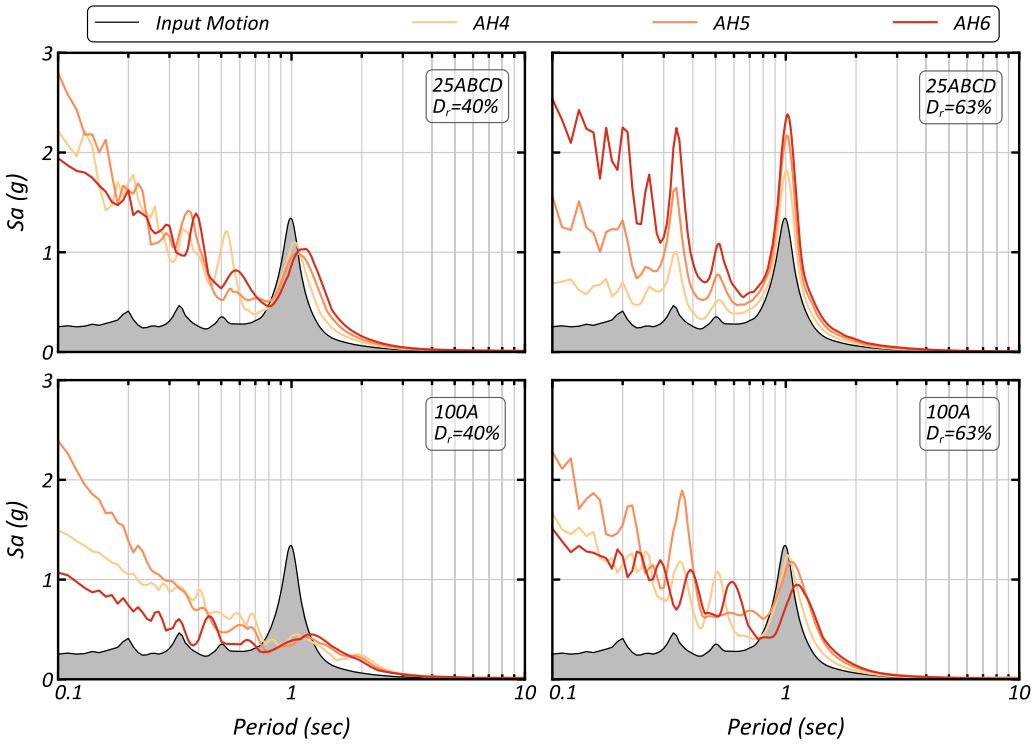

Fig. 9. Response spectra for the input motion, and shallow accelerometers beneath the level ground. Spectral acceleration responses within the shaded region are attenuated from the input motion.

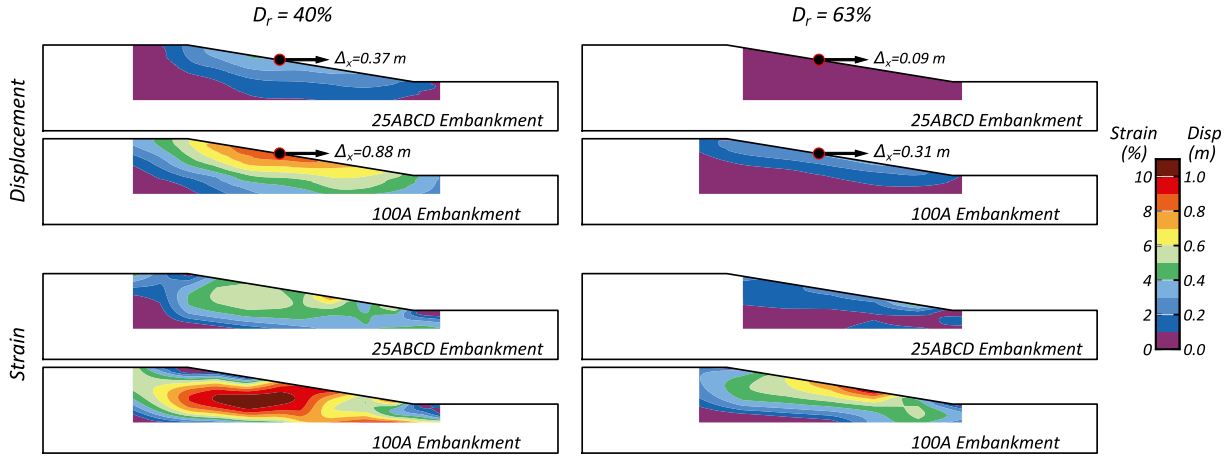

Fig. 10. Permanent displacements and shear strains from shake 3 for the $D_r = 40\%$ and $D_r = 63\%$ centrifuge model tests.

The displacements for the 25ABCD and 100A models were 0.37 m and 0.88 m, respectively.

The contours of shear strain in Fig. 10 support the displacement contours patterns and intensities. None of the embankments developed narrow bands of shear strains resulting in localized deformations. Higher shear strains were measured in the 100A embankments, consistent with the larger displacement measurements. The shear strains at the mid-depth of the 25ABCD $D_r = 63\%$ embankment ranged from 0% to 2%, while the 100A embankment strains were 5%–7%. The distribution of strains in the 25ABCD $D_r = 40\%$ embankment was unique from the 100A, $D_r = 63\%$ embankment, but the magnitudes were similar. The largest strains were measured in the 100A, $D_r = 40\%$ embankment at 10%–11%.

The in-situ sensors and high-speed cameras enable time history measurements of the permanent shear strains in Fig. 10. pseudo-elements were defined between vertically adjacent accelerometers to calculate shear stresses and strains using inverse analysis procedures from acceleration measurements (Carey et al. 2021a). A pore pressure transducer was located at the midpoint of the pseudo-elements to correlate excess porewater pressure response to changes in stress-strain behaviors. Fig. 11 shows the locations of pseudo-elements, with element 1 being beneath the level ground above the slope and element 2 in the sloping ground array. While element 1 was in the level ground, it was influenced by the global response of the system and permanent displacements did occur (See Fig. 10 for displacement contours). A pseudo-element with no biased direction of straining was not possible given the test

geometry and to provide sufficient distance between container walls to minimize boundary effects. However, it is likely permanent displacements did not accumulate until cyclic mobility and the biased straining only minimally impacted liquefaction triggering and the magnitude of dynamic strains at initial liquefaction.

In Fig. 12, the stress-strain response is given for element 1 from the $D_r = 40\%$ experiment with the excess porewater pressure response for P5 and shear strain given as a function of time. The color gradient relates the time between the different measurements, and the green ticks labeled in the upper left denote the start, hold, decay, and end phases of the input motion in Fig. 3. The cyclic stress ratio (CSR) is calculated as the cyclic shear stress in the pseudo-element normalized by the initial vertical effective confinement stress (σ'_{vo}). The points indicate the first occurrence when $r_u = 1$. The stress-strain response for 100A [Fig. 12(c)] shows several increases in shear stiffness as the soil stiffens during dilation [Fig. 12(a)] and excess porewater pressures are reduced. These increases in shear stress occur nearly simultaneously during the initial dilation spikes, and large shear strains occur [Fig. 12(e)] from 4 to 7 s. The 25ABCD sand had similar increases in cyclic stress [Fig. 12(d)] near the first occurrence of $r_u = 1$. The dilation spikes in the 25ABCD sand resulted in high magnitudes of CSR. During the period of intense shaking from 5 to 10 s, the 25ABCD soil persistently dilates and causes an increase in cyclic stresses that is not observed in the 100A sand. These increases in shear stiffness resist permanent strains, and the large unrecoverable movements did not begin to accumulate until about 10 s when the soil was no longer dilating.

The stress-strain response for element 1 for the $D_r = 63\%$ experiment is shown in Fig. 13. The higher relative density increased the number and intensity of the dilation spikes in both sands. Once $r_u = 1.0$ in the 100A embankment, dynamic strains increased to 3%. The energy at the 1 Hz frequency of the input motion was maintained in the dynamic strains for the 100A $D_r = 63\%$, consistent with the response spectrums in Fig. 9. The strong dilatancy in the 25ABCD sand produced a compact stress-strain envelope. In Fig. 13(f) the strain versus time response shows the dynamic strains increased in magnitude at a constant rate to a peak of 1% and decreased as the intensity of the input motion began to decay. The permanent strain was less than 0.25%.

The stress-strain time histories for pseudo-element 2, located within the slope (see Fig. 11 for the location), are given in Fig. 14 for all testing conditions, with the final strains matching the values in the strain contours in Fig. 10. The nonzero mean static shear stress in the slope causes a bias response, and permanent strains accumulate in the downslope direction. The static shear stress was nearly identical in all embankments. A near uniform accumulation of shear strains occurs in the 25ABCD $D_r = 40\%$ embankment during cycling. With each downslope cycle of acceleration, about 0.5% of shear strain was accumulated. The areas under these cycles were nearly uniform, suggesting mobilization of damping at a near constant rate. In the $D_r = 40\%$ 100A embankment, permanent strains irregularly accumulated, with several initial loading cycles resulting in over 6% strain. The magnitude of accumulation begins to decrease as the shaking intensity begins to decay at 12 s. The $D_r = 63\%$ 100A embankment had uniform rates of permanent

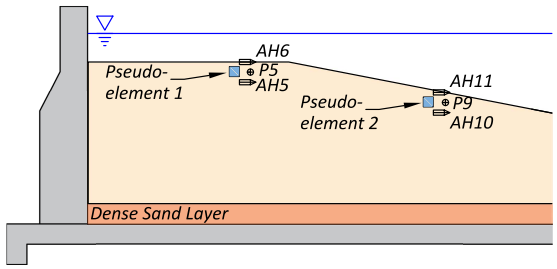

Fig. 11. Location of the pseudo-elements within the up- and mid-slope sensor arrays.

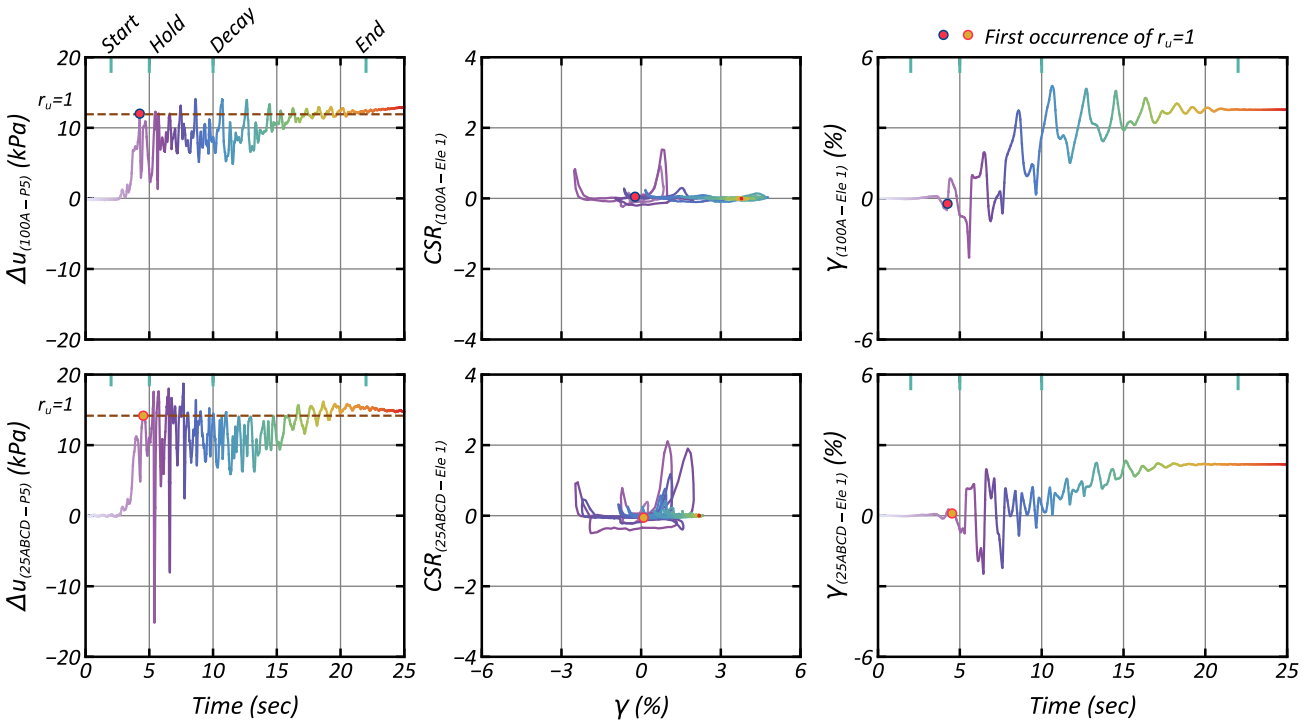

Fig. 12. Porewater pressure and stress-strain response for pseudo-element 1 (see Fig. 11 for location) measured in the $D_r = 40\%$ experiment.

J. Geotech. Geoenviron. Eng., 2023, 149(10): 04023084

Downloaded from ascelibrary.org by University Of British Columbia on 07/31/23. Copyright ASCE. For personal use only; all rights reserved.

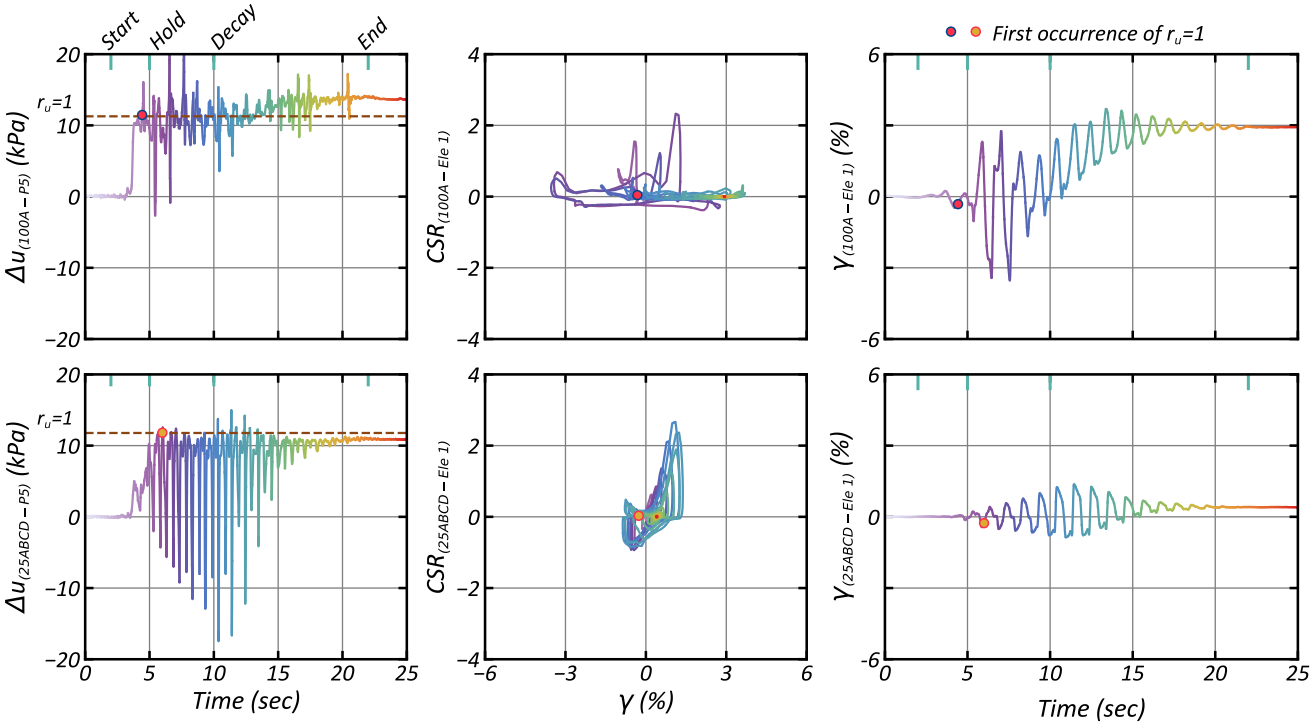

Fig. 13. Porewater pressure and stress-strain response for pseudo-element 1 (see Fig. 11 for location) measured in the $D_r = 63\%$ experiment.

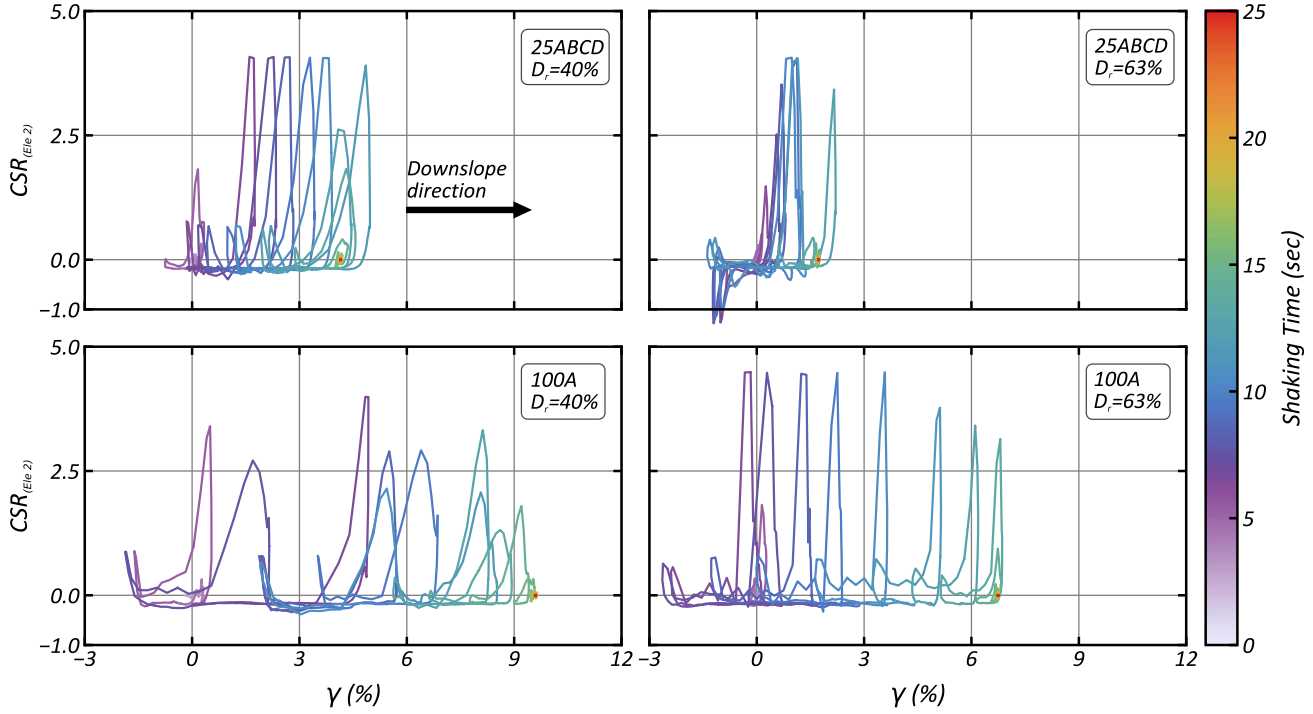

Fig. 14. Stress-strain for pseudo-element 2 (see Fig. 11 for location) for both soils and test densities.

straining during shaking, but the rate increased during later stages of loading. In the 25ABCD $D_r = 63\%$ embankment, 1%–2% shear strain accumulated during the build and hold cycles of the motion. An additional 1% of shear strain occurred during one of the decay cycles. Overall, the stress-strain responses corroborate the other measurements. While the pseudo-element may not have been located at the point of maximum strain, the patterns of strain accumulation demonstrate how the test sands have different dynamic responses.

Discussion

Findings from this centrifuge test program demonstrate that while soils may be classified as the same type, differences in gradation

Downloaded from ascelibrary.org by University Of British Columbia on 07/31/23. Copyright ASCE. For personal use only; all rights reserved.

characteristics, reflected partially by C_u, and void ratio extremes, can have impacts on the performance of geo-systems during earthquakes. While the soils in this test program were sands, it is plausible that other liquefiable broadly graded coarse-grained soils will exhibit similar or more pronounced trends as the 25ABCD sand. The observations from this work provide a rationale for the inclusion of gradation properties in the liquefaction and deformation analysis procedures.

Following standard CPT triggering relationships, liquefaction was predicted in both sands at $D_r = 40\%$ and for the 100A sand at $D_r = 63\%$. The cyclic resistance ratios (CRR) for the $D_r = 40\%$ sand were estimated at 0.12 and 0.19 for the 100A and 25ABCD sands, respectively and 0.19 for the $D_r = 63\%$ 100A sand. A CRR of 1950 was calculated for the 25ABCD sand at $D_r = 63\%$, indicating liquefaction would not trigger in this study. During testing, initial liquefaction of a $r_u = 1.0$ occurred at similar times during the input motion for both sands at each relative density. 3%–3.5% single amplitude shear strains were measured in the pseudo-elements (Figs. 12 and 13) at roughly the same time when initial liquefaction was triggered in the 100A sand, consistent with conventional coinciding definitions of liquefaction (Idriss and Boulanger 2008; Ishihara and Yoshimine 1992). Shear strains lower than 3% were measured in the 25ABCD sand at initial liquefaction for both relative densities. This suggests that excess porewater pressure and strain-based definitions of liquefaction may not be congruous for well-graded soils and that the pore pressure-based triggering evaluation will occur at a much lower shear strain. In the case of the 25ABCD sand, the excess porewater pressure triggering curve can be described using the conventional excess pore pressure-based triggering curve, while the strain criteria-based triggering curve would have a steeper slope and be shifted to the left.

Following the initial liquefaction of $r_u = 1.0$, the dynamic responses of the test sands continued to bifurcate producing different post-triggering consequences. The stress-strain responses for the pseudo-elements in the sloping ground (Fig. 14) show the 25ABCD soil accumulated less permanent strain for each cycle of downslope loading. Shear strain accumulation per cycle of loading is more constant in the 25ABCD embankments, which may result in more accurate forward numerical or analytical predictions for similar soils. The lower accumulating shear strains during cycling, and the rapid dissipation of excess porewater pressures following shaking reduced permanent displacements in the 25ABCD embankments by 0.22 and 0.52 m, or 70% and 58% from the 100A embankments for the $D_r = 63\%$ and $D_r = 40\%$ experiments, respectively.

This experimental program indicates that relative density alone may not adequately predict the dynamic performance of soils for cyclic mobility liquefaction problems. Many of the formative liquefaction studies and analysis procedures that use relative density to represent the cyclic strength of soils were developed using clean, poorly graded sands, with gradations similar to the 100A sand. Not distinguishing the dynamic response of coarse-grained soils due to differences in their physical, index, or mechanical properties may result in conservative and nonconservative design assumptions. Incorrect predictions of deformation during cyclic mobility may produce costly overdesigns or unneeded retrofits of infrastructure systems. During this testing program, it was demonstrated that the 25ABCD embankments had a 60%–70% reduction of slope surface displacements compared to the 100A embankments. It is reasonable to assume that well-graded sand or gravel would have similar or even greater resistance to displacement as the 25ABCD sand. In the case of large infrastructure projects, like earthen dams, the cost savings could be immense. Incorrectly predicting liquefaction-induced shear strains may also lead to overestimations of acceleration attenuation. In the $D_r = 63\%$ test, all spectral periods were amplified from the input motion in the 25ABCD embankment (Fig. 9). Spectral accelerations would be underestimated for the 25ABCD embankments by assuming dynamic responses are represented by 100A embankments. If these larger accelerations are not anticipated, they could damage systems located on the embankment crest.

The scope of this experimental test program is not sufficient to implement extensive changes to the liquefaction triggering and deformation procedures. It does illustrate the need for additional laboratory testing and system-level experiments that target dynamic soil behaviors identified herein. These experimental programs will better bridge the knowledge gap of how changes in physical and index properties of soil gradation directly map to deformations during liquefaction.

Summary and Conclusions

The liquefaction and cyclic mobility responses of two poorly graded sands were evaluated using centrifuge model tests. The void ratio indices and C_u of the 100A test sand was typical of the sands used for conventional liquefaction studies (Ishihara and Yoshimine 1992; Arulanandan and Scott 1993; Robertson et al. 2000; Kutter et al. 2018). The second sand, 25ABCD, had lower void ratio indices and a larger C_u, better matching the index properties of gravelly or well graded soils often encountered in natural alluvial deposits. The design of the centrifuge model test was two parallel 10-degree sloped embankments in the same model container, each constructed with different test sand but at the same relative density. These experiments show that liquefaction was triggered for both sands, but they produce different systems-level embankment performances.

The findings from this centrifuge testing program confirm that liquefaction can be triggered following an excess porewater pressure ratio criterion in sands with different gradation properties for similar seismic demands. However, these sands will have accumulated different amounts of shear strain at triggering and during cyclic mobility. As shown through this experimental program, lower amounts of strain produced in the 25ABCD sand resulted in overall lower embankment deformation. Hence, these centrifuge model tests demonstrate that the liquefaction and deformation performance of embankment systems depends on soil gradation, and a one-size-fits-all approach to understanding liquefaction-induced embankment deformations and/or displacements may not be appropriate.

The tools and procedures to estimate liquefaction-induced strains need to properly consider lower magnitudes of strain in well-graded or gravelly soils during liquefaction. This can be achieved by systematically mapping how maximum levels of strain vary for soils with different coefficients of uniformity or curvature, void ratio extremes, or novel parameters to describe the shape of gradations (i.e., Chapuis 2021). Ideally, these gradation shape parameters can be directly included in liquefaction vulnerability indices (LVIs), such as LDI or $S_{v-1\,D}$, to estimate responses with depth. A requirement for many LVI procedures is estimates of maximum shear and volumetric strains, which has been typically derived from laboratory testing on clean sands (Nagase and Ishihara 1988; Ishihara and Yoshimine 1992; Idriss and Boulanger 2008). Therefore, the current procedures may not be appropriate for well-graded or gravelly soils.

The fidelity of nonlinear constitutive models to accurately predict the dynamic behavior of well-graded soils should also be assessed. These validation routines should assess for overly and nonconservative design assumptions, like predictions of liquefaction-induced

Downloaded from ascelibrary.org by University Of British Columbia on 07/31/23. Copyright ASCE. For personal use only; all rights reserved.

deformations and embankment crest accelerations. The Liquefaction Experiments and Analysis Projects (LEAP) proposed a framework for validating numerical models predicting the effects of liquefaction through the use of laboratory element testing, and highly controlled centrifuge model tests (Carey and Kutter 2022; Kutter et al. 2018; Manzari et al. 2018). Improvement to current numerical models will produce safer geosystems and minimize costly overdesigns.

Data Availability Statement

The raw and processed data generated during this study is available via NEHRI DesignSafe-CI in the following database (PRJ-3224). The CGM data reports by Carey et al. (2021b, 2022b) provide summary figures for all sensors and shaking events for each centrifuge model test. The Python processing code generated or used during this study is available from the corresponding author by request.

Acknowledgments

The National Science Foundation (NSF) funded this work under Grant No. CMMI-1916152 and provided financial support through the Natural Hazards Engineering Research Infrastructure (NHERI) for the shared use centrifuge facility at the University of California at Davis under Grant No. CMMI-1520581. The authors would also like to thank Professors Alejandro Martinez and Katerina Ziotopoulou, Drs. Daniel Wilson, Anna Chiaradonna, Francisco Humire, Sheikh Sharif Ahmed, Ms. Rachel Reardon, and Mr. Mandeep Singh Basson, for their help with centrifuge testing, insights during data processing, and recommendations during the development of this manuscript. The assistance of the staff at the UC Davis CGM is also gratefully acknowledged.

References

Adalier, K., and A. Elgamal. 2004. "Mitigation of liquefaction and associated ground deformations by stone columns." *Eng. Geol.* 72 (3–4): 275–291. https://doi.org/10.1016/j.enggeo.2003.11.001.

Andrus, R. 1994. *In situ characterization of gravelly soils that liquefied in the 1983 Borah Peak earthquake*. Austin, TX: Univ. of Texas at Austin.

Andrus, R. D., and K. H. Stokoe II. 2000. "liquefaction resistance of soils from shear-wave velocity." *J. Geotech. Geoenviron. Eng.* 126 (11): 1015–1025. https://doi.org/10.1061/(ASCE)1090-0241(2000)126:11(1015).

Arulanandan, K., and R. Scott, eds. 1993. "Verification of numerical procedures for the analysis of soil liquefaction problems." In *Proc., Int. Conf. on the Verification of Numerical Procedures for the Analysis of Soil Liquefaction Problems*. Rotterdam, Netherlands: A. A. Balkema.

Ashford, S. A., K. M. Rollins, and J. D. Lane. 2004. "Blast-induced liquefaction for full-scale foundation testing." *J. Geotech. Geoenviron. Eng.* 130 (8): 798–806. https://doi.org/10.1061/(ASCE)1090-0241(2004)130:8(798).

ASTM. 2017. *Practice for classification of soils for engineering purposes (unified soil classification system)*. ASTM D2487-17. West Conshohocken, PA: ASTM.

Beyzaei, C. Z., J. D. Bray, M. Cubrinovski, M. Riemer, and M. Stringer. 2018. "Laboratory-based characterization of shallow silty soils in southwest Christchurch." *Soil Dyn. Earthquake Eng.* 110 (Jun): 93–109. https://doi.org/10.1016/j.soildyn.2018.01.046.

Boulanger, R. W., and I. M. Idriss. 2014. *CPT and SPT based liquefaction triggering procedures*, 138. Davis, CA: Univ. of California, Davis.

Boulanger, R. W., and I. M. Idriss. 2015. "CPT-based liquefaction triggering procedure." *J. Geotech. Geoenviron. Eng.* 142 (2): 04015065. https://doi.org/10.1061/(ASCE)GT.1943-5606.0001388.

Boulanger, R. W., M. W. Meyers, L. H. Mejia, and I. M. Idriss. 1998. "Behavior of a fine-grained soil during the Loma Prieta earthquake." *Can. Geotech. J.* 35 (1): 146–158. https://doi.org/10.1139/t97-078.

Brandenberg, S. J., D. W. Wilson, and M. M. Rashid. 2010. "Weighted residual numerical differentiation algorithm applied to experimental bending moment data." *J. Geotech. Geoenviron. Eng.* 136 (6): 854–863. https://doi.org/10.1061/(ASCE)GT.1943-5606.0000277.

Bray, J. D., and J. Macedo. 2017. "6th Ishihara lecture: Simplified procedure for estimating liquefaction-induced building settlement." *Soil Dyn. Earthquake Eng.* 102 (Aug): 215–231. https://doi.org/10.1016/j.soildyn.2017.08.026.

Bray, J. D., and F. R. Olaya. 2022. "Examination of the volumetric strain potential of liquefied soil with a database of laboratory tests." In *GeoCongress 2022: Geophysical and Earthquake Engineering and Soil Dynamics*, Geotechnical Special Publication 334, edited by A. Lemnitzer and A. W. Stuedlein, 495–505. Reston, VA: ASCE.

Cao, Z., T. Leslie Youd, and X. Yuan. 2011. "Gravelly soils that liquefied during 2008 Wenchuan, China earthquake, M_s = 8.0." *Soil Dyn. Earthquake Eng.* 31 (8): 1132–1143. https://doi.org/10.1016/j.soildyn.2011.04.001.

Carey, T., N. Love, D. Wilson, and J. DeJong. 2023. "Multi-sensor data fusion procedure for composite time history measurements in physical models." *Int. J. Phys. Model. Geotech.*

Carey, T. J., A. Chiaradonna, N. Love, J. T. DeJong, and K. Ziotopoulou. 2021a. *The effect of gradation on the response of saturated sands when subjected to seismic loading: A centrifuge test*. Niagara Falls, ON, Canada: Canadian Geotechnical Society.

Carey, T. J., A. Chiaradonna, N. C. Love, J. T. DeJong, K. Ziotopoulou, and A. Martinez. 2021b. *Effect of soil gradation on the response of a submerged slope when subjected to shaking–centrifuge data report for TJC01*, 80. Davis, CA: Univ. of California, Davis.

Carey, T. J., A. Chiaradonna, N. C. Love, D. W. Wilson, K. Ziotopoulou, A. Martinez, and J. T. DeJong. 2022a. "Effect of soil gradation on embankment response during liquefaction: A centrifuge testing program." *Soil Dyn. Earthquake Eng.* 157 (Aug): 107221. https://doi.org/10.1016/j.soildyn.2022.107221.

Carey, T. J., and B. L. Kutter. 2022. "Validation of models used to predict the effects of lateral spreading by comparison of experimental and numerical response surfaces." *Soil Dyn. Earthquake Eng.* 163 (Aug): 107379. https://doi.org/10.1016/j.soildyn.2022.107379.

Carey, T. J., N. C. Love, J. T. DeJong, K. Ziotopoulou, and A. Martinez. 2022b. *Effect of soil gradation on the response of a submerged slope when subjected to shaking—Centrifuge data report for TJC02*, 67. Davis, CA: Univ. of California, Davis.

Chapuis, R. P. 2021. "Analyzing grain size distributions with the modal decomposition method: Literature review and procedures." *Bull. Eng. Geol. Environ.* 80 (9): 6649–6666. https://doi.org/10.1007/s10064-021-02328-w.

Coulter, H. W., and R. R. Migliaccio. 1966. *Effects of the earthquake of March 27, 1964, at Valdez, Alaska*. Reston, VA: USGS.

Cubrinovski, M., J. D. Bray, C. De La Torre, M. J. Olsen, B. A. Bradley, G. Chiaro, E. Stocks, and L. Wotherspoon. 2017. "Liquefaction effects and associated damages observed at the Wellington CentrePort from the 2016 Kaikoura earthquake." *Bull. N. Z. Soc. Earthquake Eng.* 50 (2): 152–173. https://doi.org/10.5459/bnzsee.50.2.152-173.

Evans, M. D., and S. Zhou. 1995. "Liquefaction behavior of sand-gravel composites." *J. Geotech. Eng.* 121 (3): 287–298. https://doi.org/10.1061/(ASCE)0733-9410(1995)121:3(287).

Garnier, J., C. Gaudin, S. M. Springman, P. J. Culligan, D. Goodings, D. Konig, B. Kutter, R. Phillips, M. F. Randolph, and L. Thorel. 2007. "Catalogue of scaling laws and similitude questions in geotechnical centrifuge modeling." *Int. J. Phys. Modell. Geotech.* 7 (3): 01–23. https://doi.org/10.1680/ijpmg.2007.070301.

Gerolymos, N., and G. Gazetas. 2005. "Constitutive model for 1-D cyclic soil behaviour applied to seismic analysis of layered deposits." *Soils Found.* 45 (3): 147–159. https://doi.org/10.3208/sandf.45.3_147.

Ghafghazi, M., and J. T. DeJong. 2016. *A review of liquefaction case histories in gravelly soils using SPT-based triggering curves*, 8. Vancouver, BC, Canada: Canadian Geotechnical Society.

Downloaded from ascelibrary.org by University Of British Columbia on 07/31/23. Copyright ASCE. For personal use only; all rights reserved.

Downloaded from ascelibrary.org by University Of British Columbia on 07/31/23. Copyright ASCE. For personal use only; all rights reserved.

Hatanaka, M., A. Uchida, and J. Ohara. 1997. "Liquefaction characteristics of A gravelly fill liquefied during the 1995 Hyogo-Ken Nanbu Earthquake." *Soils Found.* 37 (3): 107–115. https://doi.org/10.3208/sandf.37.3_107.

Horikoshi, K., A. Tateishi, and T. Fujiwara. 1998. "Centrifuge modeling of a single pile subjected to liquefaction-induced lateral spreading." *Soils Found.* 38 (May): 193–208. https://doi.org/10.3208/sandf.38.Special_193.

Howell, R., E. M. Rathje, R. Kamai, and R. Boulanger. 2012. "Centrifuge modeling of prefabricated vertical drains for liquefaction remediation." *J. Geotech. Geoenviron. Eng.* 138 (3): 262–271. https://doi.org/10.1061/(ASCE)GT.1943-5606.0000604.

Hubler, J. F., A. Athanasopoulos-Zekkos, and D. Zekkos. 2018. "Monotonic and cyclic simple shear response of gravel-sand mixtures." *Soil Dyn. Earthquake Eng.* 115 (Aug): 291–304. https://doi.org/10.1016/j.soildyn.2018.07.016.

Idriss, I. M., and R. W. Boulanger. 2008. *Soil liquefaction during earthquakes*. Oakland, CA: Earthquake Engineering Research Institute.

Ishihara, K., and M. Yoshimine. 1992. "Evaluation of settlements in sand deposits following liquefaction during earthquakes." *Soils Found.* 32 (1): 173–188. https://doi.org/10.3208/sandf1972.32.173.

Kamai, R., and R. Boulanger. 2009. "Characterizing localization processes during liquefaction using inverse analyses of instrumentation arrays." In *Meso-scale shear physics in earthquake and landslide mechanics*, edited by I. Vardoulakis, 219–238. Boca Raton, FL: CRC Press.

Kokusho, T., T. Hara, and R. Hiraoka. 2004. "Undrained shear strength of granular soils with different particle gradations." *J. Geotech. Geoenviron. Eng.* 130 (6): 621–629. https://doi.org/10.1061/(ASCE)1090-0241(2004)130:6(621).

Kokusho, T., Y. Tanaka, K. Kudo, and T. Kawai. 1995. "Liquefaction case study of volcanic gravel layer during 1993 Hokkaido-Nansei-Oki Earthquake." In *Proc., Int. Conf. on Recent Advances in Geotechnical Earthquake Engineering and Soil Dynamics*, 9. St. Louis: Univ. of Missouri—Rolla.

Kutter, B. L. 1992. "Dynamic centrifuge modeling of geotechnical structures." *Transp. Res. Rec.* 1336 (Oct): 24–30.

Kutter, B. L. 1995. *Recent advances in centrifuge modeling of seismic shaking*, 927–942. St. Louis: Univ. of Missouri—Rolla.

Kutter, B. L., et al. 2018. "LEAP-GWU-2015 experiment specifications, results, and comparisons." *Soil Dyn. Earthquake Eng.* 113 (Feb): 616–628. https://doi.org/10.1016/j.soildyn.2017.05.018.

Kutter, B. L., et al. 2020a. "LEAP-UCD-2017 V. 1.01 model specifications." In *Model tests numerical simulations of liquefaction and lateral spreading*, edited by B. L. Kutter, M. T. Manzari, and M. Zeghal, 3–29. Cham, Switzerland: Springer.

Kutter, B. L., M. T. Manzari, and M. Zeghal. 2020b. *Model tests and numerical simulations of liquefaction and lateral spreading*. Berlin: Springer.

Kutter, B. L., and D. W. Wilson. 1999. "De-liquefaction shock waves." In *Proc., 7th US–Japan Workshop on Earthquake Resistant Design of Lifeline Facilities and Countermeasures against Soil Liquefaction*, 295–310. Buffalo, NY: Univ. at Buffalo.

Lin, P.-S., C.-W. Chang, and W.-J. Chang. 2004. "Characterization of liquefaction resistance in gravelly soil: Large hammer penetration test and shear wave velocity approach." *Soil Dyn. Earthquake Eng.* 24 (9–10): 675–687. https://doi.org/10.1016/j.soildyn.2004.06.010.

Manzari, M. T., et al. 2018. "Liquefaction experiment and analysis projects (LEAP): Summary of observations from the planning phase." *Soil Dyn. Earthquake Eng.* 113 (Aug): 714–743. https://doi.org/10.1016/j.soildyn.2017.05.015.

McCulloch, D. S., and M. G. Bonilla. 1970. *Effects of the earthquake of March 27, 1964, on the Alaska railroad*. Reston, VA: USGS.

Moss, R. E., R. B. Seed, R. E. Kayen, J. P. Stewart, A. Der Kiureghian, and K. O. Cetin. 2006. "CPT-based probabilistic and deterministic assessment of in situ seismic soil liquefaction potential." *J. Geotech. Geoenviron. Eng.* 132 (8): 1032–1051. https://doi.org/10.1061/(ASCE)1090-0241(2006)132:8(1032).

Nagase, H., and K. Ishihara. 1988. "Liquefaction-induced compaction and settlement of sand during earthquakes." *Soils Found.* 28 (1): 65–76. https://doi.org/10.3208/sandf1972.28.65.

Pires-Sturm, A. P., and J. T. DeJong. 2022. "Influence of particle size and gradation on liquefaction potential and dynamic response." *J. Geotech. Geoenviron. Eng.* 148 (6): 04022045. https://doi.org/10.1061/(ASCE)GT.1943-5606.0002799.

Robertson, P. K., et al. 2000. "The CANLEX project: Summary and conclusions." *Can. Geotech. J.* 37 (3): 563–591. https://doi.org/10.1139/t00-046.

Rollins, K. M., J. Roy, A. Athanasopoulos-Zekkos, D. Zekkos, S. Amoroso, and Z. Cao. 2021. "A new dynamic cone penetration test–based procedure for liquefaction triggering assessment of gravelly soils." *J. Geotech. Geoenviron. Eng.* 147 (12): 04021141. https://doi.org/10.1061/(ASCE)GT.1943-5606.0002686.

Rollins, K. M., J. Roy, A. Athanasopoulos-Zekkos, D. Zekkos, S. Amoroso, Z. Cao, G. Milana, M. Vassallo, and G. Di Giulio. 2022. "A new V_s-based liquefaction-triggering procedure for gravelly soils." *J. Geotech. Geoenviron. Eng.* 148 (6): 04022040. https://doi.org/10.1061/(ASCE)GT.1943-5606.0002784.

Roy, J., and K. M. Rollins. 2022. "Effect of hydraulic conductivity and impeded drainage on the liquefaction potential of gravelly soils." *Can. Geotech. J.* 59 (11): 1950–1968. https://doi.org/10.1139/cgj-2021-0579.

Ruttithivaphanich, P., and I. Sasanakul. 2022. "Liquefaction evaluation of a gravel-sand mixture using centrifuge tests." In *Geo-Congress 2022: Geophysical and Earthquake Engineering and Soil Dynamics*, Geotechnical Special Publication 334, edited by A. Lemnitzer and A. W. Stuedlein, 288–296. Reston, VA: ASCE.

Santamarina, J. C. 2003. "Soil behavior at the microscale: Particle forces." In *Soil behavior and soft ground construction*, 25–56. Reston, VA: ASCE.

Seed, H. B., I. M. Idriss, and I. Arango. 1983. "Evaluation of liquefaction potential using field performance data." *J. Geotech. Eng.* 109 (3): 458–482. https://doi.org/10.1061/(ASCE)0733-9410(1983)109:3(458).

Seed, H. B., K. L. Lee, I. M. Idriss, and F. I. Makdisi. 1975. "The slides in the san fernando dams during the earthquake of February 9, 1971." *J. Geotech. Eng. Div.* 101 (7): 651–688. https://doi.org/10.1061/AJGEB6.0000178.

Siddiqi, F. 1984. "Strength evaluation of cohesionless soil with oversize particles." Ph.D. dissertation, Dept. of Civil Engineering, Univ. of California, Davis.

Stanier, S. A., J. Blaber, W. A. Take, and D. J. White. 2016. "Improved image-based deformation measurement for geotechnical applications." *Can. Geotech. J.* 53 (5): 727–739. https://doi.org/10.1139/cgj-2015-0253.

Sturm, A. 2019. "On the liquefaction potential of gravelly soils: Characterization, triggering and performance." Ph.D. dissertation, Dept. of Civil and Environmental Engineering, Univ. of California, Davis.

Vaid, Y. P., J. M. Fisher, R. H. Kuerbis, and D. Negussey. 1990. "Particle gradation and liquefaction." *J. Geotech. Eng.* 116 (4): 698–703. https://doi.org/10.1061/(ASCE)0733-9410(1990)116:4(698).

White, D. J., W. A. Take, and M. D. Bolton. 2003. "Soil deformation measurement using particle image velocimetry (PIV) and photogrammetry." *Géotechnique* 53 (7): 619–631. https://doi.org/10.1680/geot.2003.53.7.619.

Whitman, R. V. 1971. "Resistance of soil to liquefaction and settlement." *Soils Found.* 11 (4): 59–68. https://doi.org/10.3208/sandf1960.11.4_59.

Wong, R. T., H. B. Seed, and C. K. Chan. 1974. *Liquefaction of gravelly soils under cyclic loading conditions*, 48. Berkeley, CA: Univ. of California, Berkeley.

Xu, D., H. Liu, R. Rui, and Y. Gao. 2019. "Cyclic and postcyclic simple shear behavior of binary sand-gravel mixtures with various gravel contents." *Soil Dyn. Earthquake Eng.* 123 (Sep): 230–241. https://doi.org/10.1016/j.soildyn.2019.04.030.

Youd, T. L., E. L. Harp, D. K. Keefer, and R. C. Wilson. 1985. "The Borah Peak, Idaho Earthquake of October 28, 1983—Liquefaction." *Earthquake Spectra* 2 (1): 71–89. https://doi.org/10.1193/1.1585303.